Identification of viscoplastic parameters using DIC and the virtual fields method

Stéphane Avril, Fabrice Pierron
Mechanical Engineering and Manufacturing Research Group
Ecole Nationale Supérieure d'Arts et Métiers
Rue Saint Dominique, BP508, 51006 Châlons en Champagne, FRANCE

Junhui Yan, Michael A. Sutton
Department of Mechanical Engineering, University of South Carolina,
Columbia, SC 29208, USA

ABSTRACT

In this study, tensile loading experiments are performed on 2 notched steel bars at an average applied strain rate of $1s^{-1}$. Displacement fields are measured across the specimen by coupling digital image correlation with imaging using high speed CCD cameras. Results from the experiments indicate the presence of local strain rates ranging from 0.1 to $10s^{-1}$ in the notched specimens. By coupling the virtual fields method with full-field deformation measurements at selected time intervals during the loading process, it is shown that elasto-visco-plastic constitutive parameters governing the materials behavior can be determined. Specifically, our initial studies have shown that Perzyna's model was unsuited for characterizing the transient effects detected at the onset of plasticity. However, a modified model for elasto-visco-plasticity taking account of Lüders behavior was evaluated and shown to yield promising results.

Introduction

Stresses due to inelastic deformation of materials are generally sensitive to strain rate; it is well known that the yield stress of metals increases with strain rate. Knowledge of strain rate sensitivity is necessary for accurate simulation in such situations (e.g., plastic forming, cutting).

Since experiments are needed to determine mechanical properties for simulations, an appropriate visco-plastic constitutive model describing the mechanical behavior of materials sensitive to strain rates is employed [1]. Simple mechanical experiments (i.e., tension and/or compression of prismatic specimens; torsion of thin tubes) may be carried out. For experiments performed under quasi static conditions, the specimens generally have relatively uniform stress and strain distribution in the gage area of the specimen. By increasing the velocity of the applied displacement/loading, resulting in strain rate increases within the specimen, material parameters governing the visco-plastic behavior can be identified. For example, by plotting the different values of yield stress obtained at different strain rates, an appropriate yield stress vs strain rate model can be defined.

Though simple in concept, this experimental approach has two main drawbacks. First it requires a large number of experiments performed at different strain rates. Second, the assumption of uniform strain and stress distribution is only satisfied under quasi-static conditions; for strain rates $\geq 1\ s^{-1}$, transient strain localization effects cannot be avoided in the specimen. Thus it is not possible to ensure that the strain rate and the stress are constant in the gage length of the specimen.

It will be shown in this study that localization effects can be used as an asset if the spatially and temporally varying displacement fields is measured at appropriate time intervals throughout the specimen. Indeed, heterogeneity of strain rate implies that different strain rates occur at different positions in the same specimen, which implies that the measured displacement fields may provide sufficient information for identifying the constitutive parameters governing the elasto-visco-plastic behavior of the material.

The measurement of displacement fields, even at moderately high strain rates, is feasible today with modern high speed camera systems [2]. The widespread use of digital image correlation (DIC), and its coupling with the technology of high-speed cameras, can provide the desired displacement fields. However, the data processing towards the final aim of identifying material constitutive parameters remains an issue.

Pioneers in this area of research for elasto-plastic behavior were Meuwissen and his coworkers [3]. They suggested performing experiments leading to non uniform stress states, with the idea of retrieving more parameters from a single, well-characterized experiment. The parameters are retrieved by calibrating a finite element (FE) model against the measured displacement fields. This approach is very powerful as the number of parameters identified in a single experiment can be much larger than in classical tensile or torsion loading experiments. Kajberg and his coworkers recently extended this approach to elasto-visco-plastic behavior [4-5]. However, one of the main drawbacks is that FE computation is time consuming; estimating a few parameters from experimental data can easily take more than 20 hours in some cases [6].

A much faster approach for identifying elasto-plastic constitutive parameters from full-field measurements, which does not require any FE computations, has been suggested recently. Originally developed for the identification of elastic properties [7-9], the virtual fields method (VFM) was validated for the identification of elasto-plastic constitutive parameters on simulated data by Grédiac and Pierron [10] and then on experimental data by Pannier et al. [11]. To use the VFM for estimating elasto-plastic material parameters, the measured displacement fields are used to quantify the stress components across the specimen. Since the resulting stresses depend upon parameters in the constitutive model via the stress-strain relationships, by requiring the stresses to satisfy equilibrium constraints (via the principle of virtual work), the input material parameters are updated until the equilibrium is satisfied.

This study is an extension of the VFM to elasto-visco-plasticity. A tensile loading experiment has been specifically designed to give rise to heterogeneous stresses and strain rates across a flat thin bar made of mild steel (very sensitive to strain rate). In the following sections, the experiments are described and the principle for identifying the elasto-visco-plastic constitutive parameters is presented.

Classical characterization of elasto-visco-plasticity

The material used in the experiments is 99.5% pure iron. 'The specimen is machined from a 2mm thick sheet into a dog-bone shape, with straight edges over a gage length of 60mm. All of the specimens were cut in the rolling direction of one single metal sheet so as to avoid a variation of mechanical properties due to the anisotropy induced by rolling[1]. In order to provide reference values for the constitutive parameters, the material was characterized at different strain rates (2×10^{-4} s^{-1}, 4.2×10^{-2} s^{-1}, 1.05×10^{-1} s^{-1}, 2.5×10^{-1} s^{-1}, 4.2×10^{-1} s^{-1} and 1.05 s^{-1}) by standard tensile loading experiments on coupons, using 3 samples at each strain rate.

The stress-strain curves obtained from the standard tensile loading experimnets are linear before yielding. Young's modulus $E=$ 199 GPa is deduced from the slope of the curves and is independent of strain rate. Poisson's ratio $\nu =$ 0.30 was characterized only at 2×10^{-4} s^{-1} using strain gage rosette measurements.

The stress-strain curves after yielding are non linear. The Von Mises yield function is assumed to be relevant here (isotropic behavior) for modeling the elastic limit of the material. The Von Mises effective stress, denoted $\underline{\sigma}$, is defined as:

$$\underline{\sigma} = \sqrt{\frac{3}{2}\sum_{i,j} S_{ij}S_{ij}} \tag{1}$$

where: S is the deviatoric stress tensor with components S_{ij} defined like:

$$S_{ij} = \sigma_{ij} - \frac{1}{3}\delta_{ij}\sum_{k}\sigma_{kk} \tag{2}$$

The Von Mises yield surface, which defines the elastic limit for a material under multiaxial loading, contains all stress components such as $\underline{\sigma} = \sigma_e$, where σ_e is the flow stress. In order to take hardening into account, the flow stress σ_e may be linked to the effective plastic strain, denoted p, and defined as:

[1] Data for a tensile loading experiment performed at a strain rate of 2×10^{-4} s^{-1} indicates that the material properties in the transverse and rolling directions are similar, suggesting isotropy in material response is a reasonable approximation.

$$p = \int_{history} \sqrt{\frac{2}{3}\dot{\varepsilon}^p : \dot{\varepsilon}^p} \tag{3}$$

where: $\dot{\varepsilon}^p$ is the plastic strain rate tensor, with components $\dot{\varepsilon}_{ij}^p$.

In a standard uniaxial tensile loading experiment, the effective plastic strain may be derived according to:

$$p = \varepsilon - \frac{\sigma}{E} \tag{4}$$

where: ε is the total strain component in the direction of tension and σ is the stress component in the direction of tension derived from the resultant load.

Using the experimental tensile loading results for the present material, the relationship between flow stress σ_e and effective plastic strain has been fitted, in the range $0<\varepsilon<0.03$, by a linear model of the form:

$$\sigma_e(p) = Y_0 + E_t p \tag{5}$$

where: Y_0 is the initial yield stress and E_t is the linear hardening modulus.

It can clearly be seen from the results of Tab. 1 that E_t and Y_0 depend on the strain rate. The present study focuses only on the initial yield stress. It is very sensitive to the strain rate, showing that the investigated material has a visco-plastic behavior.

The rate dependent model chosen here for coupling Y_0 and the strain rate is the one suggested by Perzyna [1,4], in which the plastic strain rate is given by:

$$\dot{p} = \gamma \left\langle \frac{Y_0}{\sigma_0} - 1 \right\rangle^n = \gamma \left\langle \frac{\sigma - E_t p}{\sigma_0} - 1 \right\rangle^n \tag{6}$$

where σ_0 is the quasi-static initial yield stress, γ is the strain rate sensitivity and n is the over stress exponent; $\langle X \rangle = X$ if $X>0$, $\langle X \rangle = 0$ otherwise. The values deduced for this model using the data from Table 1 are: σ_0 = 140 MPa, γ = 0.5 s^{-1} and n = 8.

Tab. 1. Reference values for the yield stress and hardening modulus at different strain rates.

Strain rate	2×10^{-4} s^{-1}	4.2×10^{-2} s^{-1}	0.105 s^{-1}	0.25 s^{-1}	0.42 s^{-1}	1.05 s^{-1}
Y_0	190 MPa	249 MPa	255 MPa	267 MPa	279 MPa	296 MPa
R_0	2400 MPa	970 MPa	960 MPa	830 MPa	770 MPa	700 MPa

Novel approach for identifying elasto-visco-plastic constitutive parameters

Experiment and specimen

A tensile loading experiment was specifically designed to give rise to heterogeneous distributions of stresses and strain rates across a flat thin specimen. Fig.1a shows the notched bar tensile specimen. The initial displacement ramp rate is ≈ 61 mm/s. The data sampling rate for recording the resultant load applied by the MTS tensile machine is 1000 Hz. Two high speed cameras were used for synchronized recording of images of the front and back surfaces of a nominally planar specimen; images of each surface are required so that data measured on both sides could be averaged out to remove the parasitic effects of out-of-plane motion on the deformation measurements [11]. Imaging was performed at 4796 frames per second with full resolution of 800×600 pixels.

Deformation of the specimen during loading was analyzed by the DIC technique with the help of VIC-2D software [12] using a 21×21 pixel correlation window and a step size of 5 pixels between subset centers. Image correlation measurements are estimated to have a positional error of ≈ 10^{-2} pixel.

Experiments were performed with two specimens. For filtering purpose, the measured displacement fields were projected on a basis of piecewise linear functions, denoted f_k [9]. The geometry of the specimen was meshed using triangles (Fig.1b). Each function f_k equals one at a given node of the mesh and zero at all the other nodes. The reconstructed displacement fields can be written:

$$\begin{cases} U_x(x,y) = \sum_k a_k f_k(x,y) \\ U_y(x,y) = \sum_k b_k f_k(x,y) \end{cases} \tag{7}$$

where a_k and b_k were obtained by regression in the least squares sense. Then, the displacement fields reconstructed with the basis functions were used to deduce the strain fields required for the identification, with an estimated strain accuracy of 2.10^{-5}.

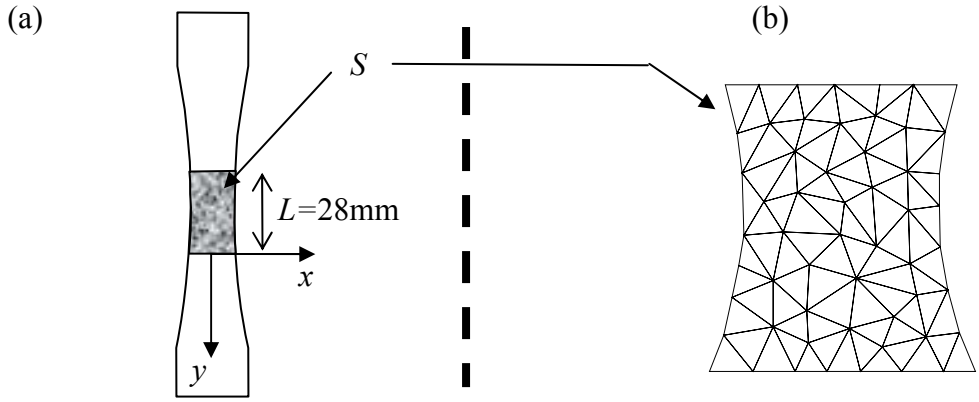

Figure 1. (a) Specimen. (b). Measurement area meshed with triangles for reconstruction of displacement fields

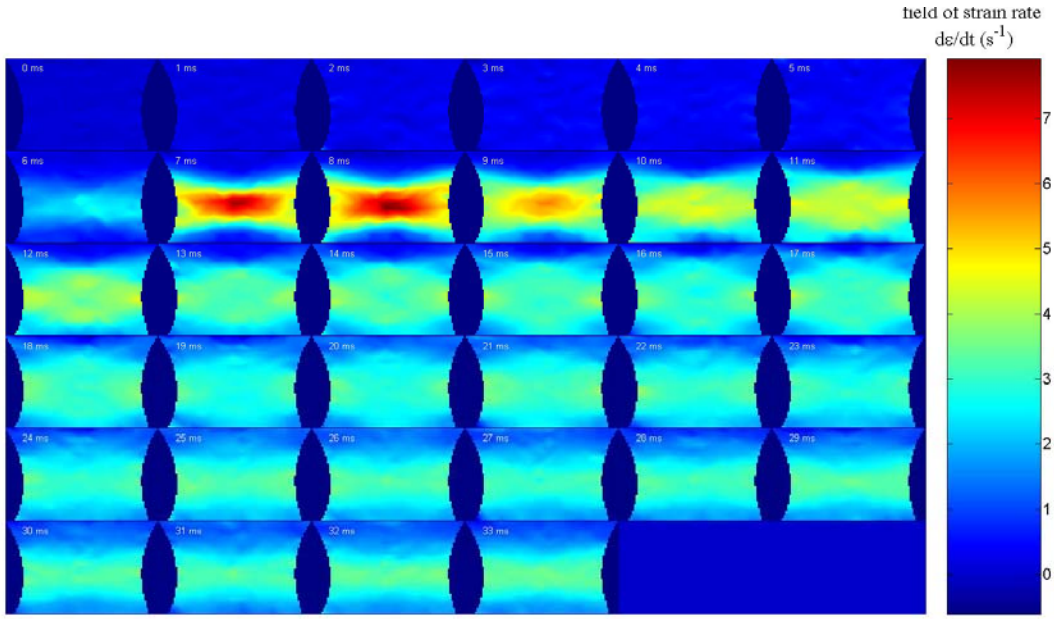

Figure 2: Strain rate fields during experiment.

Differentiating the ε_{yy} strain field with time provides maps of the strain rate $d\varepsilon_{yy}/dt$ (see Figure 2). Interestingly, the strain rate fields are heterogeneous, varying between 0.01 s^{-1} and 8 s^{-1}, even though the far-field displacement rate is held constant throughout the experiment. Since the same phenomenon was observed at all strain rates, the following discussion is provided.

First, high values of strain rate are clearly observed in the center of the specimen ≈ 7ms after initiating the displacement ramp (see Figure 2), in agreement with the visco-plastic model in Eq (2). Indeed, the plastic strain rate is directly linked to the effective stress and the distribution of the effective stress is similar to the distribution of strain rate shown at 7ms, with a peak at the center of the specimen. Second, since the plastic strain rate is a power function of $(Y_0/\sigma_0 - 1)$ with a large exponent, the plastic strain rate begins increasing when Y_0 reaches $2\sigma_0$. Physically, this feature of the model is related to dislocation motion at the microscale; dislocations cannot move at the prescribed speed if the applied stress is not sufficient. Third, when $Y_0 > 2\sigma_0$ the plastic strain rate in the center part of the specimen overtakes the local prescribed strain rate that occurred during the elastic stage, inducing a redistribution of strains and also a decrease of the measured resultant load (see Figure 3). Large strain rates in the center of the specimen are compensated by a quasi-zero strain

rate away from the center. Therefore, for the same ramping rate of the tensile machine, much larger strain rates could be reached because only a localized part of the specimen continues to be deformed. The transition from a quasi-uniform strain rate distribution during the elastic behavior to a localized strain rate distribution after the onset of plasticity provides conditions for characterizing the visco-plastic behavior in a single experiment. The following section shows how the strain fields can be processed to get the constitutive parameters governing this behavior.

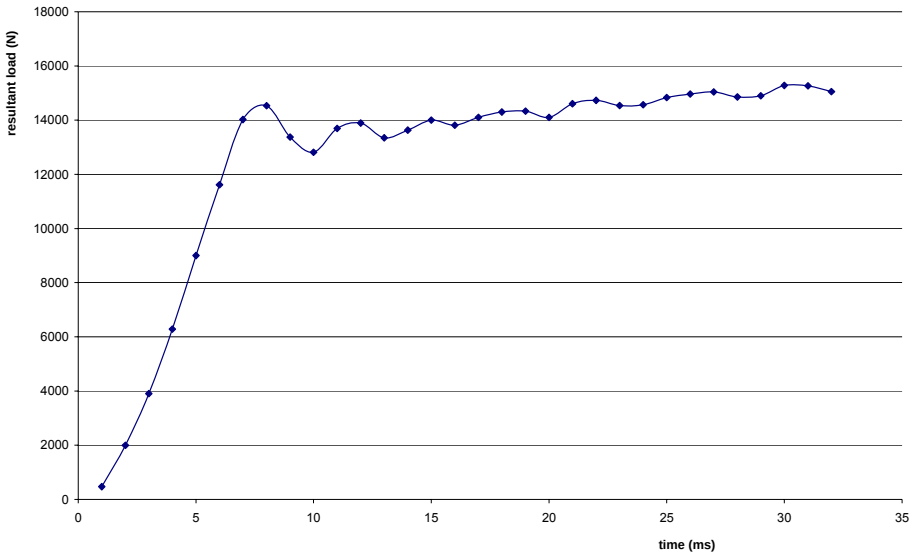

Figure 3: Measured resultant load during experiment

The virtual fields method in the elastic range

The global equilibrium of a solid with no body forces acting on it can be written like:

$$-\sum_{i,j}\int_{V}\sigma_{ij}\varepsilon_{ij}^{*}dS+\sum_{i}\int_{\partial V}T_i u_i^{*}dS=0 \qquad (8)$$

This equation is referred to as the "principle of virtual work". The σ_{ij} are the component of the stress tensor across the volume of the solid (denoted V), the T_i are the components of the traction vector applied over the external surface of the solid (denoted ∂V), the u_i^{*} are the components of a vectorial test function which only has to be continuous across the solid. This test function is named "virtual displacement field" and the ε_{ij}^{*} are the components of the virtual strain tensor derived from it.

Let us assume that the investigated specimen is in a plane stress state. This is relevant due to the thinness of the plate, its constant thickness (denoted t in the following) and due to the applied loading (in-plane tension). Thus the stress can be assumed as homogeneous across the thickness, along with the strain and the deformation.

Before yielding (the elastic behavior range lasts ≈ 6ms), the material is elastic and isotropic. During this time, the stress components can be expressed as a linear function of the strain components (using the convention of contracted indices ($xx\rightarrow x$, $yy\rightarrow y$, $xy\rightarrow s$):

$$\begin{pmatrix}\sigma_x\\ \sigma_y\\ \sigma_s\end{pmatrix}=\frac{E}{1-\nu^2}\begin{bmatrix}1 & \nu & 0\\ \nu & \nu & 0\\ 0 & 0 & \frac{1-\nu}{2}\end{bmatrix}\begin{pmatrix}\varepsilon_x\\ \varepsilon_y\\ \varepsilon_s\end{pmatrix} \qquad (9)$$

Thanks to the measurement of the displacement fields and their projection on the basis of piecewise linear function shown in Eq (7), the in-plane strain fields are known across a whole area of interest in the specimen. Writing Eq. (3) over this area, one has:

$$\frac{E}{1-\nu^2}\left[\int_{S}\left(\varepsilon_x\varepsilon_x^{*}+\varepsilon_y\varepsilon_y^{*}+\frac{1}{2}\varepsilon_s\varepsilon_s^{*}\right)dS+\nu\int_{S}\left(\varepsilon_y\varepsilon_x^{*}+\varepsilon_x\varepsilon_y^{*}-\frac{1}{2}\varepsilon_s\varepsilon_s^{*}\right)dS\right]=\frac{1}{t}\int_{\partial V}T_i u_i^{*}dS \qquad (10)$$

The latter equation is satisfied with any virtual field u_i^* [7]. Poisson's ratio is identified by using a virtual field that minimizes noise effects and for which the contribution of the resultant load is cancelled [9].

Young's modulus is identified using: $u_x^* = 0$ and $u_y^* = y$, corresponding to the following virtual strain field: $\varepsilon_{xx}^* = 0$ and $\varepsilon_{yy}^* = 1$ and $\varepsilon_{xy}^* = 0$. For this choice of virtual field, Eq. (5) with this virtual field can be written in the form,

$$\frac{E}{1-\nu^2}\left[\int_S \varepsilon_y dS + \nu \int_S \varepsilon_x dS\right] = \frac{PL}{t} \tag{11}$$

where L is the length of the area of interest where the measurement is achieved (see Fig. 1a) and P is the measured load resultant.

The area of the surface of interest where the measurement is achieved is denoted S. Defining $\underline{\varepsilon_x}$ and $\underline{\varepsilon_y}$ as the average strains over the area of interest S, one gets:

$$\frac{E}{1-\nu^2}(\underline{\varepsilon_y} + \nu \underline{\varepsilon_x}) = \frac{PL}{St} \tag{12}$$

Young's Modulus is identified by plotting $P(\tau_l)L/St$ (average stress) versus $(\underline{\varepsilon_x}(\tau_l) + \nu\, \underline{\varepsilon_y}(\tau_l))/(1 - \nu^2)$ (dimensionless, like strains), all along the experiment (where τ_l denotes time frames, τ_l, $0<l<N$). The obtained curve is eventually fitted by a linear curve in the elastic domain for estimate E.

The virtual fields method in the plastic range

To analyze material behavior in the domain of plasticity, and in agreement with the visco-plastic model of Eq. (2), one has to define the flow rule, which derives from the yield surface according to Hill's principle of normality. It indicates the direction of the plastic strain rate tensor. According to Perzyna's model of viscoplasticity [1], it is written like:

$$\dot{\varepsilon}_{ij}^p = \frac{3}{2}\dot{p}\frac{S_{ij}}{\sigma_e} = \frac{3}{2}\gamma\left(\frac{\underline{\sigma} - E_t p}{\sigma_0} - 1\right)^n \frac{S_{ij}}{\sigma_e} \tag{13}$$

Actually, in practice, all the strain rates are approximated by their increment between two frames: $\dot{\varepsilon} = \Delta\varepsilon / T$, where T is the time between two frames. Eventually, the flow rule can be written:

$$\Delta\varepsilon_{ij}^p = \frac{3}{2}\gamma\left(\frac{\underline{\sigma} - E_t p}{\sigma_0} - 1\right)^n \frac{S_{ij}}{\sigma_e} \tag{14}$$

The strain decomposition rule has also to be introduced. It can be written:

$$\Delta\varepsilon = \Delta\varepsilon^{elast} + \Delta\varepsilon^p \tag{15}$$

where: $\Delta\varepsilon$ is the measured strain increment between two frames, $\Delta\varepsilon^{elast}$ is the elastic strain increment between two frames and $\Delta\varepsilon^p$ is the plastic strain increment between two frames.

Using Eq. (14) and (15), it is possible to compute the elastic and plastic strains during the experiment from both: the available full-field measurements in the area of interest, and a given set of constitutive parameters σ_0, n, γ, E_t, E and ν. The full procedure is based on Eqs.(9) and (14) to relate stresses to elastic and plastic strains, respectively, and Eq. (15) to relate elastic and plastic strains. A similar procedure was developed by Sutton and his coworkers within the framework of elasto-plasticity [13]. Their algorithm has been modified and implemented within the framework of Perzyna's elasto-visco-plasticity. It provides the stress fields during the loading process from the available full-field measurements in the measurement area.

Using these stress fields, it is possible to the suitability of the parameters σ_0, n, γ, E_t input into the algorithm. Parameters E and ν are deduced from the strain fields measured before the onset of plasticity and therefore, one only needs to check the suitability of σ_0, n, γ, E_t during the post-elastic deformation process. This is achieved simply by applying the principle of virtual work written in Eq.(11), with: $u_x^* = 0$ and $u_y^* = y$, but considering only the elastic part of the strain.

Accordingly, the following equation should be verified at each time τ during the experiment:

$$\int_S \sigma_y(\sigma_0, n, \gamma, E_t, \tau) dS = \frac{P(\tau)L}{t} \tag{16}$$

Since experimental noise in the data will introduce errors in Eq (16), the idea is to compute iteratively the stress fields with the procedure mentioned above and to update σ_0, n, γ, E_t until the minimum of the following cost function is reached:

$$F(\sigma_0, n, \gamma, E_t) = \int_{\tau=0}^{end} \left(\frac{1}{S} \int_S \sigma_y(\sigma_0, n, \gamma, E_t, \tau) dS - \frac{P(\tau)L}{St} \right)^2 \quad (17)$$

Equation (17) is the quadratic deviation between the average longitudinal stress computed from the measured displacement fields and the average longitudinal stress computed from the measured resultant load, integrated over the duration of the experiment. The evolution of both average stresses has been plotted in Figure 4 at the minimum of the cost function. This minimum is generally reached in about 50 iterations by using a Nelder-Mead algorithm (≈ 2 minutes of time computation using a Pentium M, 1400 MHz). This represents a dramatic reduction of the computation time compared to use of finite element model updating approaches that require several hours to obtain similar results [6].

Results and discussion of Perzyna's model

The material parameter obtained using the approach presented in the previous sections are reported in Table 2. The estimated material parameters are obtained for each specimen by using the two sets of data obtained from separate high speed cameras on each side of the specimen to independently compute the parameters. The results are compared with the reference.

Tab. 2. Results obtained using the procedure described above to identify Perzyna's model parameters

	E (GPa)	ν	σ_0 (MPa)	E_t (GPa)	γ (s^{-1})	n
Spec. 1, Cam. 1	203	0.27	156	0.40	0.16	19
Spec. 1, Cam. 2	203	0.32	156	0.80	0.48	10.1
Spec. 2, Cam. 1	198	0.30	145	0.38	0.15	10.4
Spec. 2, Cam. 2	198	0.32	152	0.14	0.22	13.6
Reference	199 ±4	0.3 ±0.02	140	< 0.7	0.5	8

Regarding elastic parameters, the Young modulus identified on both sides of the two specimens are the same and in agreement with the reference. Regarding the Poisson's ratio, discrepancies exist between both sides of the same specimen (Tab. 2). Since Young's modulus is the same on both sides, it can be concluded that bending effects and out of plane parasitic motions discussed by Pannier et al. [11] are negligible in these experiments and are not responsible for the measured discrepancies in Poisson's ratio. Based on our preliminary evaluation, it is difficult to explain these discrepancies and it is conjectured that the combination of data scattering and the cost function used for optimization may be responsible for the variations.

Regarding the visco-plastic parameters, Table 2 shows that there is general agreement with the reference values for σ_0 but deviations from the reference values remain large for parameters such as γ and n. The hardening modulus has no counter part in the reference experiments because the localized strain rates reached in the notched bar could not be reached in the dog-bone specimen. Nevertheless, it is noted that the values of E_t identified in the notched bars are always lower than the ones identified in the dogbone specimens. This trend is in agreement with a reduction of hardening as strain rate increases, as shown in Table 1.

Deviations for γ and n may be explained by different reasons. Reference experiments cover only a few decades of strain rates, with only six different values. This may be insufficient to accurately estimate the three parameters in Perzyna's model. Experiments carried out on the notched bars with a full-field measurement technique provide richer information, as each triangle defined in the measurement area (Figure 1b) corresponds to an independent measurement. Such a density of data can be used to assess the relevancy of Perzyna's model when used to model material behavior. This was achieved by comparing the evolution of average stress deduced from the displacement fields (using optimal values of σ_0, n, γ, E_t) with the average stress obtained from the resultant load. It can be deduced from Figure 4a that, even at the minimum of cost function F, poor agreement exists between the average stress deduced from the resultant load and the average stress computed from the displacement fields; oscillations of the resultant load could not be reproduced from the displacement fields. More detailed investigation by the authors indicates that no set of values could be found for σ_0, n, γ, E_t that would result in displacement fields where such oscillations occur.

Accordingly, Perzyna's model in Eq. (6) seems unsuited to model the observed behavior; it is unclear whether the Nelder-Mead algorithm converged to a global minimum of cost function F for the Perzyna model.

The unsuitability of Perzyna's model may account for errors obtained for exponent n in Table 2. Indeed, the cost function is only sensitive to this parameter at the onset of plasticity, between 6ms and 9ms, when the distribution of strain rates is the widest (varying between 0.01 s^{-1} and 8 s^{-1}, according to the maps plotted in Figure 2). As the model is unsuited during this part of the experiment (it cannot provide similar oscillations for the stresses deduced from the displacement fields), it is unlikely that the exponent n in Table 2 can be correctly estimated. For the same reason, values reported in Table 2 for the hardening modulus are probably lower than expected for strain rates of less than 10 s^{-1}.

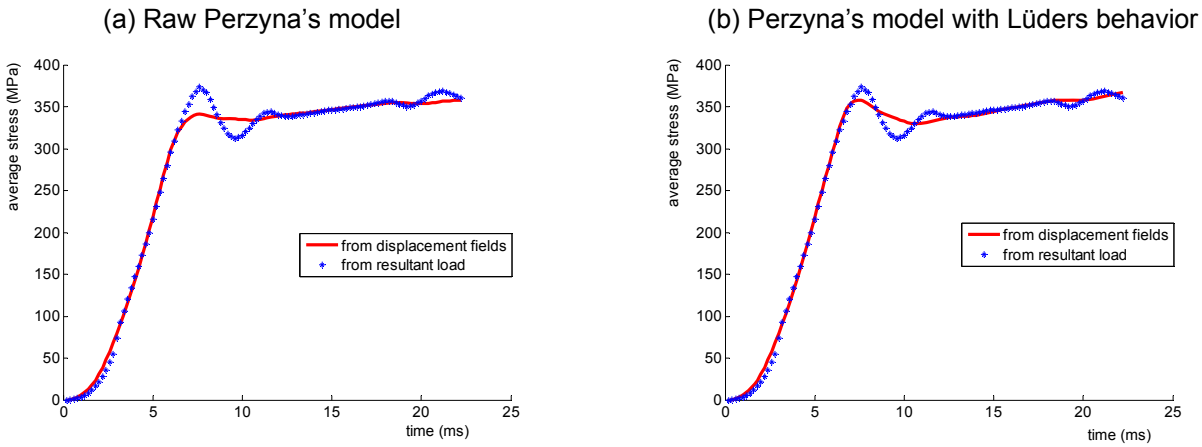

Figure 4: Average stress curves obtained from the measured displacements fields (Spec. 2, Cam. 1) for identifying the elasto-visco-plastic constitutive parameters.

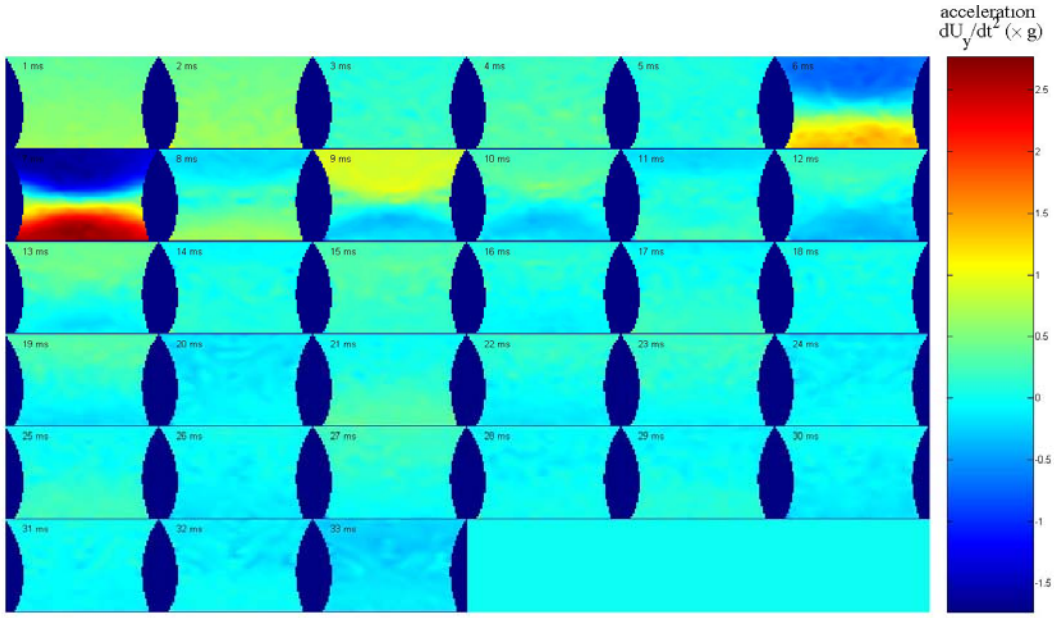

Figure 5: Field of vertical acceleration (direction of loading).

Results with an improved model taking account of Lüders behavior

As shown in Figure 4a, results using Perzyna's model are roughly in agreement with the values obtained from the displacement fields, except in the transient part when oscillations occur. To account for this particular behavior in the transient part, the zone of localized strain rate in Figure 2 may actually be viewed as a Lüders

band. Lüders bands occur usually in annealed mild steel at any strain rates and even in non-annealed mild steel at high strain rates [14,15]. Sharp yield points and subsequent abrupt yield drops were noticed at the highest strain rates of the standard tests, but not for the lower strain rates. This phenomenon results from the rapid multiplication of mobile dislocations and the stress-dependence of dislocation velocity. It induces the initiation of bands at the shoulder corners of dog-bone specimens in standard tests. Afterwards, the bands move towards the center of the specimen and eventually the strain recovers its uniformity. It is different in our specimen because, due to the specimen geometry, the Lüders bands are unable to escape from the notched zone [16]. Then, it just disappears when the dislocation multiplication ends.

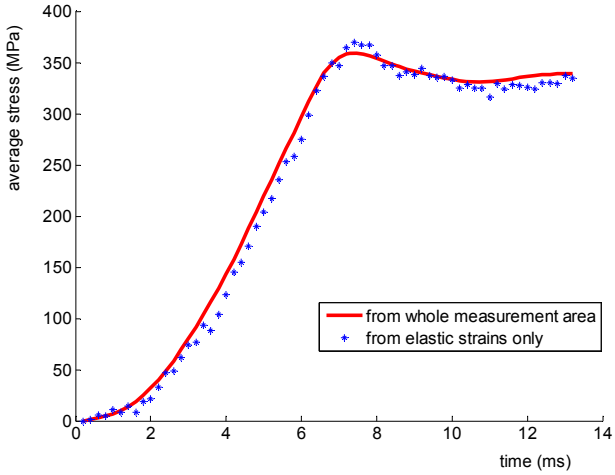

Figure 6: Average stress curves obtained from the measured displacements fields (Spec. 2, Cam. 1) using the whole measurement zone or only the cross section at the top which remains fully elastic.

In order to model this effect, one has to consider that γ in Eq. (13) or (14) depends on the cumulative plastic strain p [14,15]. Indeed, γ is the product of the number of dislocations by the elementary velocity of each dislocation (the Burgers vector). If the number of mobile dislocations changes, γ cannot be assumed as constant. A general model suited for Lüders behavior is the Yoshida's model [14,15]. It may be written:

$$\gamma = \gamma_\infty + (\gamma_0 - \gamma_\infty)e^{-\lambda p} \tag{18}$$

Therefore, let us consider the following model as an extension of Perzyna's model to loading configuration where the plastic strain increment may vary very fast:

$$\dot{p} = \left[\gamma_\infty + (\gamma_0 - \gamma_\infty)e^{-\lambda p}\right]\left\langle \frac{\underline{\underline{\sigma}} - E_t p}{\sigma_0} - 1 \right\rangle^n \tag{19}$$

where: λ, γ_0 and γ_∞ are 3 constants to determine.

If λ is close to zero, the material is almost not affected by the Lüders effect and Perzyna's usual model is recovered. Using Eq (18) instead of the usual Perzyna model for deriving stresses from the measured displacements, one obtains improved agreement in the transient stage. For example, the curve deduced from displacement fields in Figure 4b was deduced with parameters: σ_0 = 134 MPa, γ_0 = 0.007 s^{-1}, γ_∞ = 0.2 s^{-1}, E_t = 1.6 GPa, n = 5.4 and λ = 26. These parameters are the ones for which the best agreement between both curves in Figure 4b is reached.

Even though the new model provides a nice drop of the average stresses after the onset of plasticity, discrepancies remain: there is no oscillation after the drop in the average stress deduced from the displacement fields whereas oscillations are recorded by the load cell. Actually, the oscillations recorded by the load cell are probably induced by vibrations in the tensile machine, affecting only the load cell data (far-field stress) but not the stresses in the field. Indeed, a large energy release results from the occurrence of the Lüders band at the onset of plasticity. Significant accelerations (computed from the displacement fields by a double differentiation along the time) can be observed in the measurement area at this moment (at 7 ms in Figure 5). The bottom of the specimen has an acceleration of more than 2.5g (25 m/s^2) and the top accelerates in the backward direction at about -1.5g (-15 m/s^2). Vibrations are induced by this sudden acceleration and this result in a reverse acceleration field at 9 ms: the bottom now accelerates backward and

the top forward, as if a shock wave was coming back after being reflected at the cross head of the tensile machine. These vibrations are amplified at the load cell due to the mass of the cross heads and other machine components. Indeed, if a mass of 40 kg was accelerated at 2.5g, the load would be amplified by 1000 N, and thus the average stress deduced from the resultant load would be amplified of 25 MPa. This is beyond the remaining discrepancy between both curves in Figure 4b.

Therefore, the load cell data cannot be used for our approach during the transient zone of the test, between 6 ms to 15 ms, because there is a discrepancy between the far-field stresses (at the load cell) and the stresses in the measurement area due to the vibrations. Fortunately, the cross section at the top of the measurement area remains elastic during the whole duration of the transient effects (6 ms to 15 ms). Accordingly, the average stress of this elastic cross section is easily deduced from the measured strain, as it only depends on E and ν, which have already been identified. It is plotted in Figure 6. As expected, there is a drop at the onset of plasticity, but no oscillation is visible because the mass of the specimen is too small to induce any significant inertial effect here.

The elastic stress at the top of the measurement area can be compared to the average stress of the whole measurement area deduced with our approach. The model taking account of Lüders behavior is still used instead of the classical Perzyna's model because one has to recover the drop in the curve. Results show a very good agreement between both average stresses in Figure 6. Thus, the model given in Eq (19) is relevant for the actual yield flow in the studied material. This shows also that the requirement of using a load cell can be removed if the elastic properties of the material are known. Indeed, the strains measured through a given cross section of the material can be used to derive the stresses through this cross section, and the resultant load can be deduced directly from the total stresses through this cross section, which replaces the load cell.

It is important to point out that the model which has been calibrated in this study takes account of strain localization transient effects induced at the onset of plasticity. This is only possible by coupling a full-field measurement technique and an inverse approach. Transient phenomena are usually not considered by authors who attempt calibration of visco-plastic constitutive models using global response data. By using full-field data, our results confirm that the transient component of the visco-plastic constitutive response can be modeled so that an aspect of the actual visco-plastic behavior of metals that may be of importance at high strain rates can be adequately characterized.

Conclusions

In this paper, the identification of elasto-visco-plastic constitutive parameters from full-field deformation measurements was investigated. The shape of the specimen was selected in order to provide non uniform strain rate conditions within the specimen. Using the strain rate heterogeneity, strain fields measured on this single specimen have been shown to provide sufficient information to adequately characterize the elasto-visco-plastic behavior of a typical strain-rate sensitive material using a combination of the virtual fields method with full-field deformation measurements. Specifically, the parameters identified with this approach were compared with the ones obtained using dog-bone specimens. Discrepancies were noticed for the Perzyna's model, due to transient localization effects occurring at the onset of plasticity which were not adequately represented by Perzyna's model. Promising results were obtained using a modified version of Perzyna's functional form taking account of Lüders behavior.

The procedure proposed herein for quantification of elasto-visco-plastic model parameters, which requires a combination of full-field deformation measurements and an appropriate computational methodology to ensure overall equilibrium and satisfaction of boundary conditions, allows investigators to address the issue of transient strain localization at the onset of plasticity in tensile experiments carried out at a high strain rate. Extension to very high strain rates is one of the main prospects for this approach because the transient effects would be augmented. The recent drastic improvements in the technology of high-speed cameras will soon provide suitable conditions for these experiments.

References

1. Lemaître, J. and Chaboche, J.L. *Mechanics of Solid Materials*. Cambridge University Press, 1990.
2. Schreier, H. and Sutton, M. Systematic errors in digital image correlation due to undermatched subset shape functions. *Experimental Mechanics*, 42(3):303-310, 2002. Springer.

3. Meuwissen, M.H.H., Oomens, C.W.J., Baaijens, F.P.T., Petterson, R., and Janssen, J.D. Determination of the elasto-plastic properties of aluminium using a mixed numerical-experimental method. *Journal of Materials Processing Technology*, 75:204–211, 1998.
4. Kajberg, J., Wikman B. Viscoplastic parameter estimation by high strain-rate experiments and inverse modelling – Speckle measurements and high-speed photography. *International Journal of Solids and Structures*, 44:145–164, 2007.
5. Kajberg, J., Sundin, K.G., Melin, L.G., Stahle, P. High strain-rate tensile testing and viscoplastic parameter identification using microscopic high-speed photography. *International Journal of Plasticity*, 20:561–575, 2004.
6. Kajberg, J., Lindkvist G. Characterisation of materials subjected to large strains by inverse modelling based on in-plane displacement fields. *International Journal of Solids and Structures*, 41:3439–3459, 2004.
7. Grédiac, M. Principe des travaux virtuels et identification. *Comptes Rendus de l'Académie des Sciences*, 309:1-5, 1989.
8. Grédiac, M., Toussaint, E., and Pierron, F. Special virtual fields for the direct identification of material parameters with the virtual fields method. 1- Principle and definition. *International Journal of Solids and Structures*, 39(10):2691-2706, 2002. Elsevier.
9. Avril, S., and Pierron, F. General framework for the identification of constitutive parameters from full-field measurements in linear elasticity. *International Journal of Solids and Structures*, in press, 2007. Elsevier.
10. Grédiac, M. and Pierron, F. Applying the virtual field method to the identification of elasto-plastic constitutive parameters. *International Journal of Plasticity*, 22:602-627, 2006.
11. Pannier, Y., Avril, S., Rotinat, R., and Pierron, F. Identification of elasto-plastic constitutive parameters from statically undetermined tests using the virtual fields method. *Experimental Mechanics*, in press, 2006.
12. www.correlatedsolutions.com.
13. Sutton, M.A., Deng, X., Liu, J., and Yang, L. Determination of elastic plastic stresses and strains from measured surface strain data. *Experimental Mechanics*, 36(2):99-112, 1996.
14. Sun, H.B., Yoshida, F., Ma, X., Kamei, T., and Ohmori, M. Finite element simulation on the propagation of Lüders band and effect of stress concentration. *Materials Letters*, 57:3206-3210, 2003.
15. Yoshida, F. A constitutive model of cyclic plasticity. *International Journal of Plasticity*, 16:359-380, 2000.
16. Graff, S., Forest, S., Strudel, J.-L., Prioul, C., Pilvin, P. and Béchade, J.-L. Strain localization phenomena associated with static and dynamic strain ageing in notched specimens: experiments and finite element simulations. *Materials Science and Engineering A*, 387-389:181-185, 2004.